Synopsis:
Analysis of a Metallic Specimen

OAK RIDGE National Laboratory

Introduction

The All-Domain Anomaly Resolution Office (AARO) sponsored a series of measurements on a layered material specimen primarily composed of magnesium and zinc, with bands of bismuth and other co-located trace elements. The material specimen, whose origin and purpose are of long and debated history, is claimed to be recovered from an unidentified anomalous phenomenon (UAP) crash in or around 1947. Furthermore, the specimen's physiochemical properties are claimed to make the material capable of "inertial mass reduction" (i.e., levitation or antigravity functionality), possibly attributable to the material's bismuth and magnesium layers acting as a terahertz waveguide.

Previously, US Army Combat Capabilities Development Command (DEVCOM) established a Cooperative Research and Development Agreement (CRADA) with To the Stars Academy (TTSA) to evaluate the feasibility of exploiting any potential disruptive technology associated with this widely discussed specimen.

AARO, founded in 2022, is congressionally mandated to explore historical records of UAP incidents and publicly report its findings. Although the long chain of custody for this specimen cannot be verified, public and media interest in the specimen warranted a transparent investigation that adhered to the scientific method. Subsequent to the TTSA–DEVCOM CRADA, AARO secured science and technology partner Oak Ridge National Laboratory (ORNL), one of 17 US Department of Energy national laboratories, to independently assess and perform thorough characterization studies on the specimen, leveraging ORNL's 80-year history of world-leading materials science expertise.

Figure 1. View of the as-received bulk specimen. Sticker containing internal sample tracking information edited out for public release.

ORNL, an expert in materials characterization, has the diverse staff expertise and co-located, powerful instrumentation suites to allow rigorous scientific inquiry beyond the capabilities of most individual laboratories. Therefore, it is a highly qualified institution to maintain scientific integrity in its unbiased analysis of this specimen and its properties.

AARO tasked ORNL with assessing whether (1) the specimen is of terrestrial origin and (2) the bismuth in the specimen could act as a terahertz waveguide. DEVCOM Ground Vehicle System Center provided ORNL access to the metallic specimen—a single parent sample and three previously derived subsamples, all from the same material—beginning in February 2023.

ORNL materials science analyses evaluated the sample's structure, chemical composition, and isotope ratios via multiple methods, including microscopy, spectroscopy, and spectrometry. Results align with previous DEVCOM analyses, indicating that the structure and composition of the bismuth layers do not meet the requirements necessary to serve as a terahertz waveguide. Furthermore, all data strongly support that the material is terrestrial in origin.

Methods

All analyses and materials utilization were authorized and overseen by TTSA via the DEVCOM CRADA, and all analyses were preapproved by AARO and DEVCOM before ORNL received the specimen.

Morphology and microstructural characteristics were investigated using the following techniques.

- Optical microscopy: standard microscope analysis that allows imaging of microstructural features.
- Computerized tomography, aka CT scan: X-ray imaging procedure that produces a 3D image of a sample without damaging it, revealing interior structural features.
- Scanning electron microscopy–energy dispersive x-ray spectroscopy (SEM-EDS): technique that produces 2D images at higher resolution to allow analysis of microstructure and elemental makeup.
- (Scanning) transmission electron microscopy–energy dispersive x-ray spectroscopy ([S]TEM-EDS): a suite of techniques that pass a high-energy (e.g., 200 kV) electron beam through a thin (<200 nm) foil of sample, allowing analysis of crystal structure, grain and feature morphology, and defects, as well as elemental makeup, all with nanometer to subnanometer resolution.

Analyses of bulk chemical, elemental, and isotopic composition used mass spectrometry techniques, a suite of widely used analytical techniques that identify elements, their abundance within a sample (including very trace quantities), and their isotopic composition.

Traceable quality control standards and method blanks were run throughout all analyses to monitor sample integrity and instrument performance.

Results

Morphology and Structure

Data are consistent across multiple imaging approaches, showing that the material consists of distinct layers that merge and diverge at various points throughout the material.

Interfaces showed fractures and other features that ORNL determined are consistent with a material that was originally whole but was strained by heat exposure and mechanical forces, possibly for extended periods. Figure 2 shows images of the specimen constructed using CT.

ELEMENT	AVERAGE
Bi	3813
Pb	2859
Tl	215.13
Fe	55.1
Cd	36.96
Mn	28.99
Au	10.618
Mo	0.5922
Sn	0.1328
Ba	0.0465

Units: trace elements are in parts per million (micrograms per gram of sample)

Table 1. Trace element composition of the specimen (sans the bulk magnesium-zinc matrix), in decreasing order of abundance. All are considered "trace," at less than 0.1% abundance. Gray reflects results from inductively coupled plasma optical emission spectroscopy (ICP-OES); Blue reflects results from high-resolution ICP-MS.

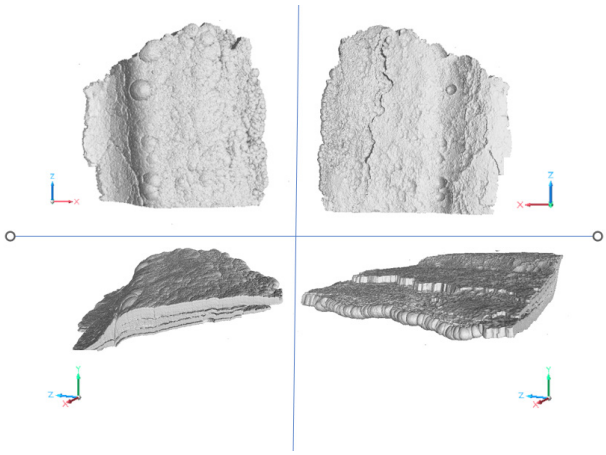

Figure 2. Images produced via CT showing multiple angles of the bulk specimen, showcasing features including the layer nature of the material (bottom left) and edge with probable heat damage (bottom right).

Chemical Composition

Analysis using SEM-EDS determined that magnesium and zinc are the primary elements present in the specimen, comprising approximately 97.5% and 2% of the material, respectively. Minor elements detected (Table 1) were lead (Pb) and bismuth (Bi) (Figure 3), with lesser trace amounts of iron (Fe) and manganese

(Mn). Inductively coupled plasma mass spectrometry (ICP-MS), the most sensitive analysis technique performed, additionally revealed the presence of small amounts of cadmium (Cd), thallium (Tl), gold (Au), molybdenum (Mo), tin (Sn), and barium (Ba). If a detected element abundance fell beneath the lower bound of the calibration curve or below the method detection limit, then the element is not displayed in Table 1 because that element was extremely unlikely to have been a purposeful addition to the manufacturing process.

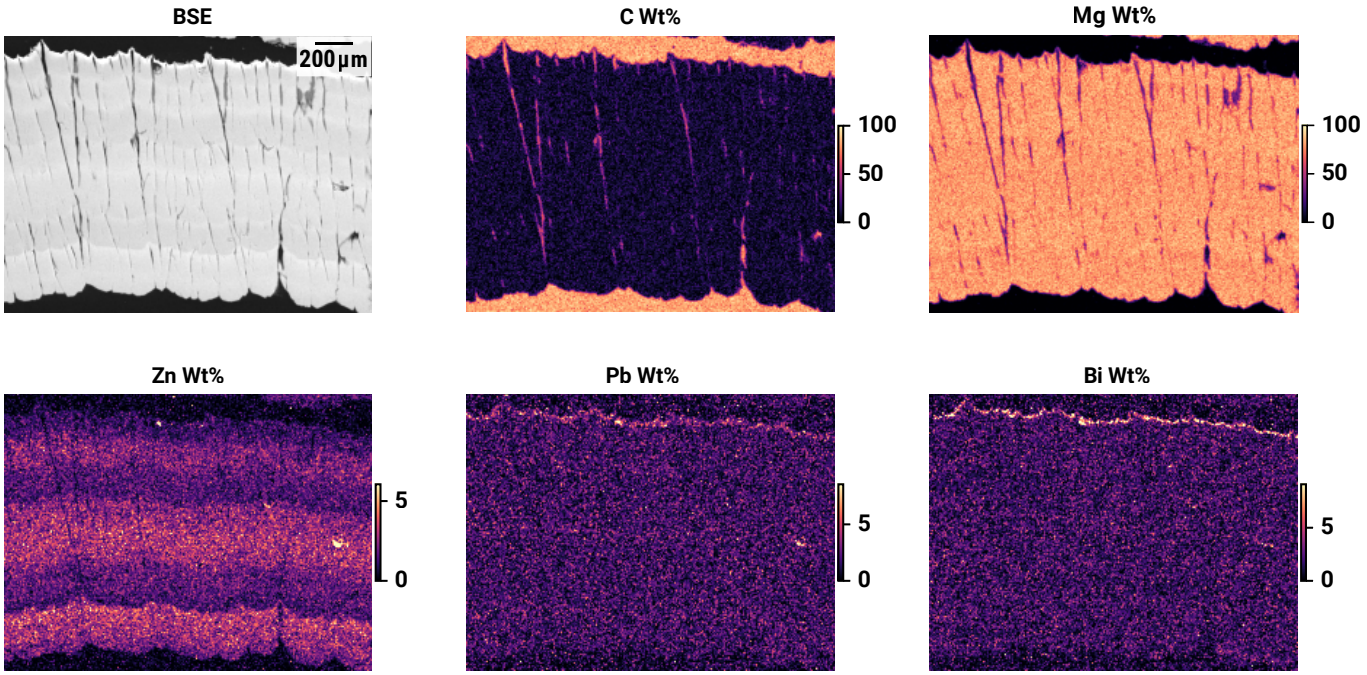

Figure 3: Backscattered electron image (BSE, top left) and energy dispersive x-ray spectrometry (EDS) maps from one subsample (SEM beam energy: 30 kV), presented as estimated weight percent (minor elements not shown, so numbers will not total 100%). Carbon (C) map indicates the embedding epoxy. The magnesium matrix (Mg) is clearly visible, along with the cracks in the matrix. The zinc (Zn) map shows regions of higher and lower zinc content. At the top of the lead (Pb) and bismuth (Bi) maps, co-located layers are visible. (Figure 5 presents additional imaging of the banded element composition, showing multiple Pb–Bi layers.)

Crystalline Structures

TEM revealed that the crystalline structure of magnesium in the specimen was consistent with common magnesium alloy structures (Figure 4). Laser ablation ICP-MS revealed banding of the zinc components, along with layered co-location of lead and bismuth (in an approximate 1:1 ratio) in the bands. The bismuth-rich portions of the specimen lacked a clear crystalline structure, instead appearing to consist of highly nanocrystalline pockets in an otherwise amorphous matrix (Figure 4).

Pure single-crystalline bismuth in a single thin layer has been postulated to have the ability to function as a waveguide, a material that can disrupt or direct an electric or energy field—in this case, terahertz waves (electromagnetic waves with microscale wavelengths). Although the damage to the specimen (including suspected heat stress) precludes a definitive statement describing the specimen's original structure, the amorphous and nanocrystalline appearance of the bismuth in the examined layers of the current specimen likely indicates that a pure crystalline layer of bismuth was never present within the material.

Moreover, the postulated structure of such a theoretical bismuth-based waveguide requires it to be in a single layer between a material possessing a different dielectric constant. However, multiple bismuth layers throughout a material have not been postulated to be capable of achieving or improving this waveguide functionality—in fact, multiple layers could instead interfere with such functionality. Thus, the layered nature of the impure bismuth within the specimen likely precludes it from acting as a waveguide (Figure 5).

Finally, based on the postulated hypothetical uses of bismuth, the dielectric properties necessary for bismuth to function as a waveguide would have been disrupted in this material because the bismuth in the specimen is co-located and mixed with lead (Figures 3 and 5). Based on these findings ORNL determined that this material is highly unlikely to have ever functioned as a bismuth-based terahertz waveguide.

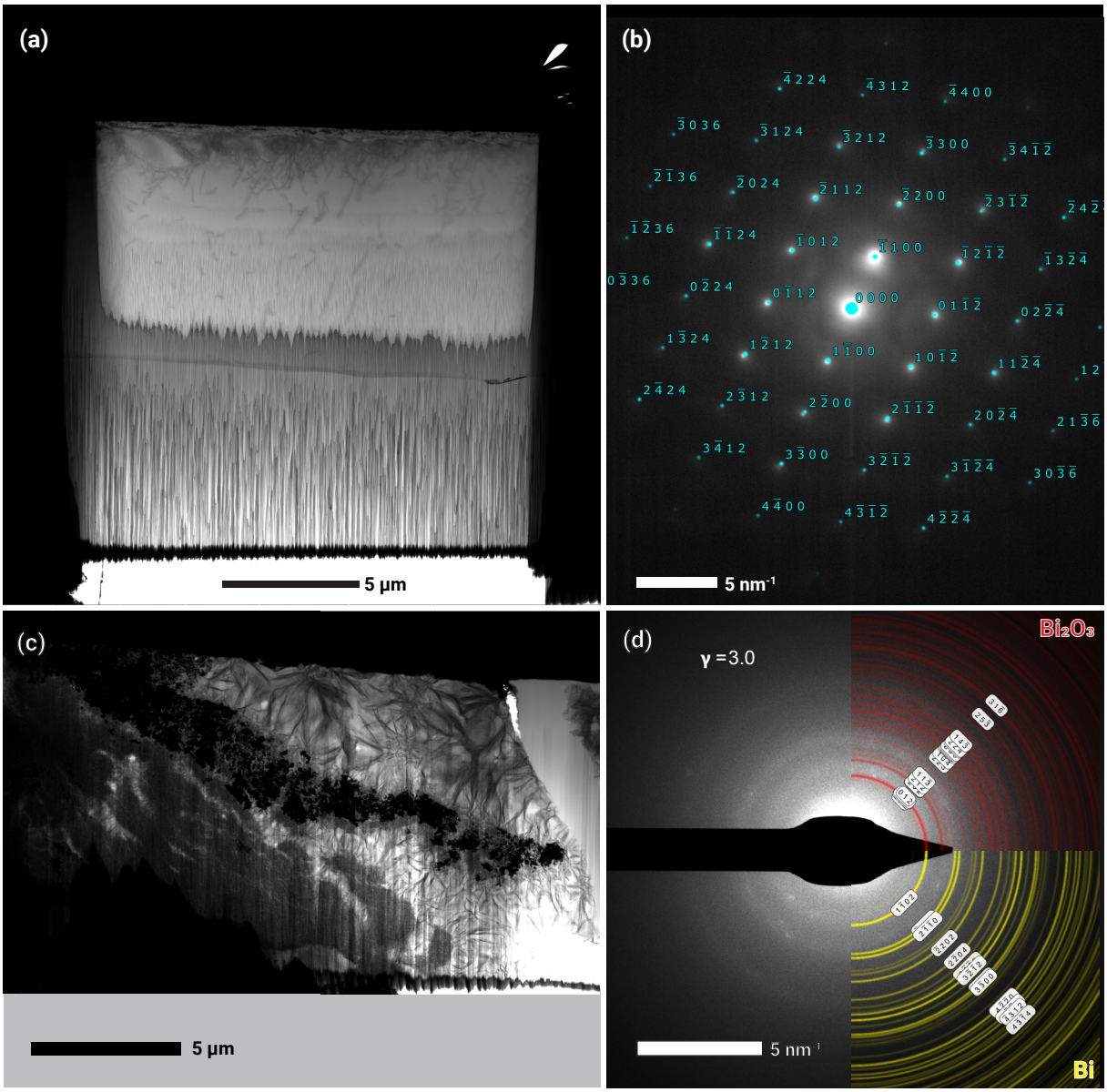

Figure 4: (a) TEM micrograph of a single-crystalline region from the bulk of the sample; structural defects are visible at this level of resolution (this figure is showing an area that represents just 2 to 3 pixels of the area shown in Figure 3). The vertical lines at the bottom are a focused ion beam preparation artifact. (b) Selected area electron diffraction pattern (SAEDP) from the region in (a), indexed to the standard Mg structure. (c) A low-magnification montage TEM micrograph of an area showing a dense bismuth-rich layer (dark central band). (d) A SAEDP from a bismuth-rich band. The electron diffraction pattern (with image processing γ=3.0) from the bismuth-rich region is shown in the white rings. Both bismuth (Bi, yellow) and Bi_2O_3 (red) calculated ring patterns are shown for comparison; Bi is a slightly better match. The diffraction indicates that the bismuth layer is nanocrystalline and highly defective.

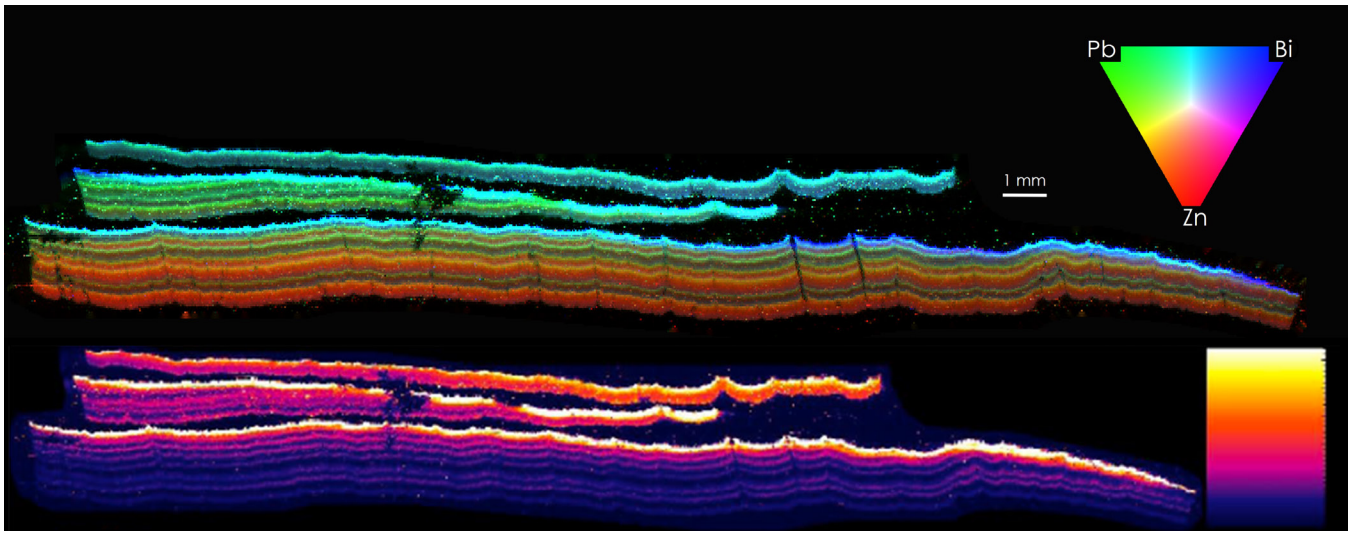

Figure 5. Laser ablation ICP-MS elemental maps. (Top) Colocation of lead (green), bismuth (blue), and zinc (red), the three primary minor elements in the material. Blending of colors indicates co-location: teal indicates the nearly 1:1 ratio of lead to bismuth. (Bottom) Elemental map of bismuth concentration (hot [yellow] = more, cool [purple] = less). Bismuth is most concentrated at the top but is present in many repeating layers.

Isotope Analysis

Multicollector ICP-MS analysis showed that the specimen's magnesium and lead isotope composition is consistent with other materials manufactured and used terrestrially (Figures 6 and 7). Isotopes are varying forms of the same element with differing mass, and their proportions affect the chemical properties of and reveal information about the history of the material within which the isotopes are found. All elements have isotopes, and the ratio between the amounts of various isotopes is called the isotopic signature, which is akin to a fingerprint in chemical analyses.

The magnesium isotopic signature of the specimen is fractionated (possibly owing to the mechanical and heat strain that the material appears to have undergone) but falls within normal terrestrial compositions and precisely within the expected trendlines of fractionation (Figure 6). Each star system has a magnesium isotopic composition that was inherited from its local star-forming region. Figure 6 shows the magnesium isotopic signature of various materials originating within our solar system. The straight lines in the bottom graphic representation are the kinetic and equilibrium mass fractionation trendlines, which define the types of isotopic shifts incurred on the basis of mass. Fractionation occurs due to chemical reactions and physical processes (e.g., manufacturing and mining) and is normal during the lifespan of natural and manufactured materials and their components. The materials in Figure 6—including the specimen—fall on or near the fractionation trendlines, strongly indicating that their starting compositions were once the same and have been systematically changed as a result of mass fractionation. If a material originated outside our solar system, its magnesium isotopic signature could plot nearly anywhere in the top graphic representation of Figure 6—instead, the specimen's data plots it precisely within the expected fractionation trendlines for known compositions specific to our solar system.

Less complexly, the lead isotopic signature of this specimen is fully consistent with "common lead" compositions that exist naturally on Earth and within terrestrial materials (Figure 7), distinctly separate from even lunar materials, indicating it is extremely likely that the material originated on Earth.

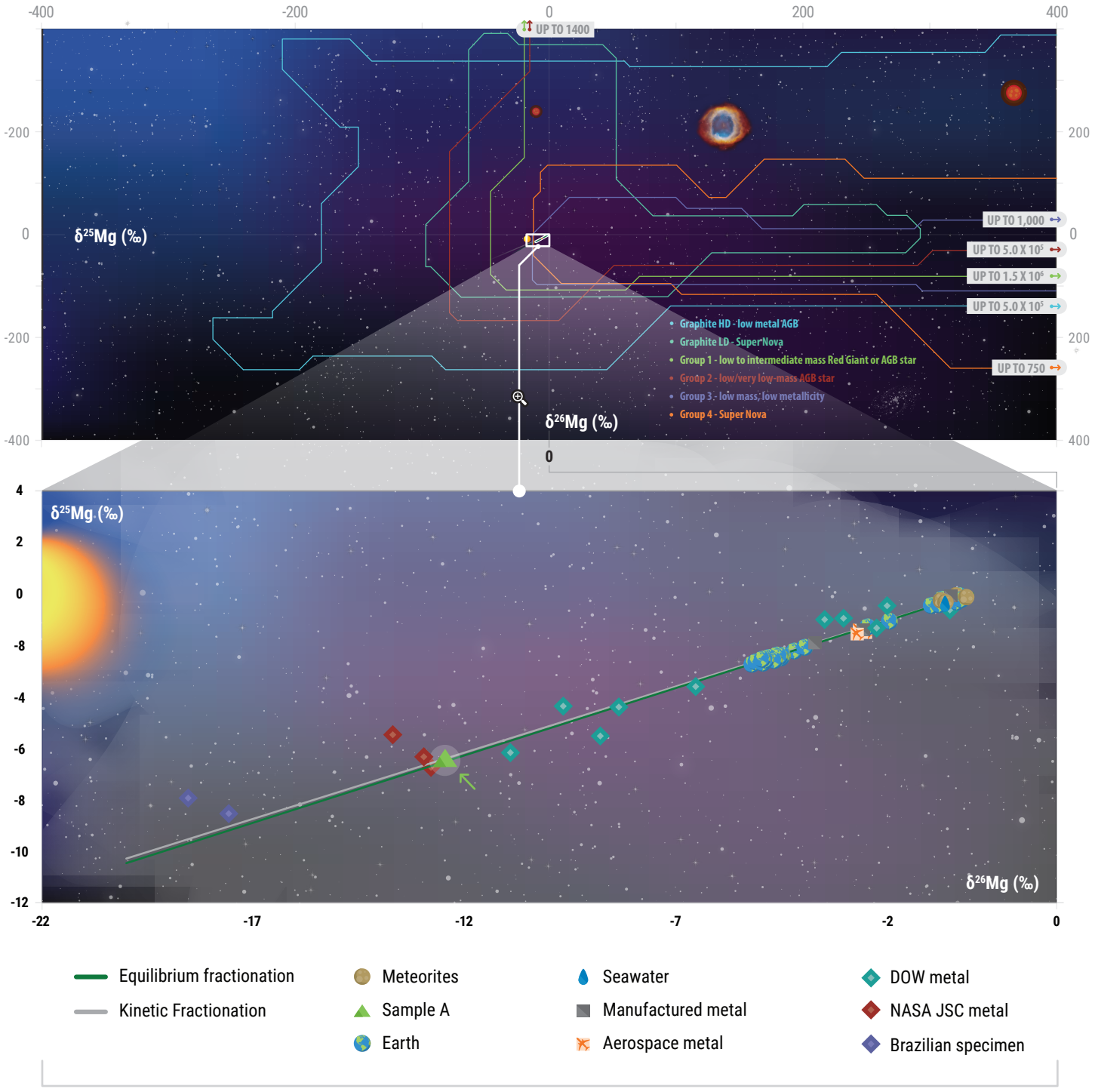

Figure 6: Artistic representation including the magnesium isotope systematics of the unknown material, specifically shown relative to other terrestrial, non-terrestrial, and extrasolar materials. The figures plot the $\delta^{26}Mg'$ vs. the $\delta^{25}Mg'$, which represent the differences in $^{26}Mg/^{24}Mg$ and $^{25}Mg/^{24}Mg$ isotopes relative to a known standard (DSM-3) in parts per thousand (‰) notation. This calculation adjusts for known instrumental mass bias effects inherent in ICP-MS analyses and is consistent with how magnesium data in literature are often presented. (Top) The extreme magnesium isotope compositions possible from different star types. (Bottom) A zoomed-in view of the magnesium isotope compositions of local solar system materials and the material in question. Uncertainty envelopes are not included, but when plotted with their uncertainties, data points overlap the kinetic and equilibrium fractionation lines. (Note: Data points shown with a diamond shape, included for completeness, were extracted from an older analysis source; we cannot directly verify the precision or correctness of these data. The delta values were calculated relative to DSM-3, and a systematic offset correction factor was applied; error bars for these points reach ± 2 ‰ uncertainty.)

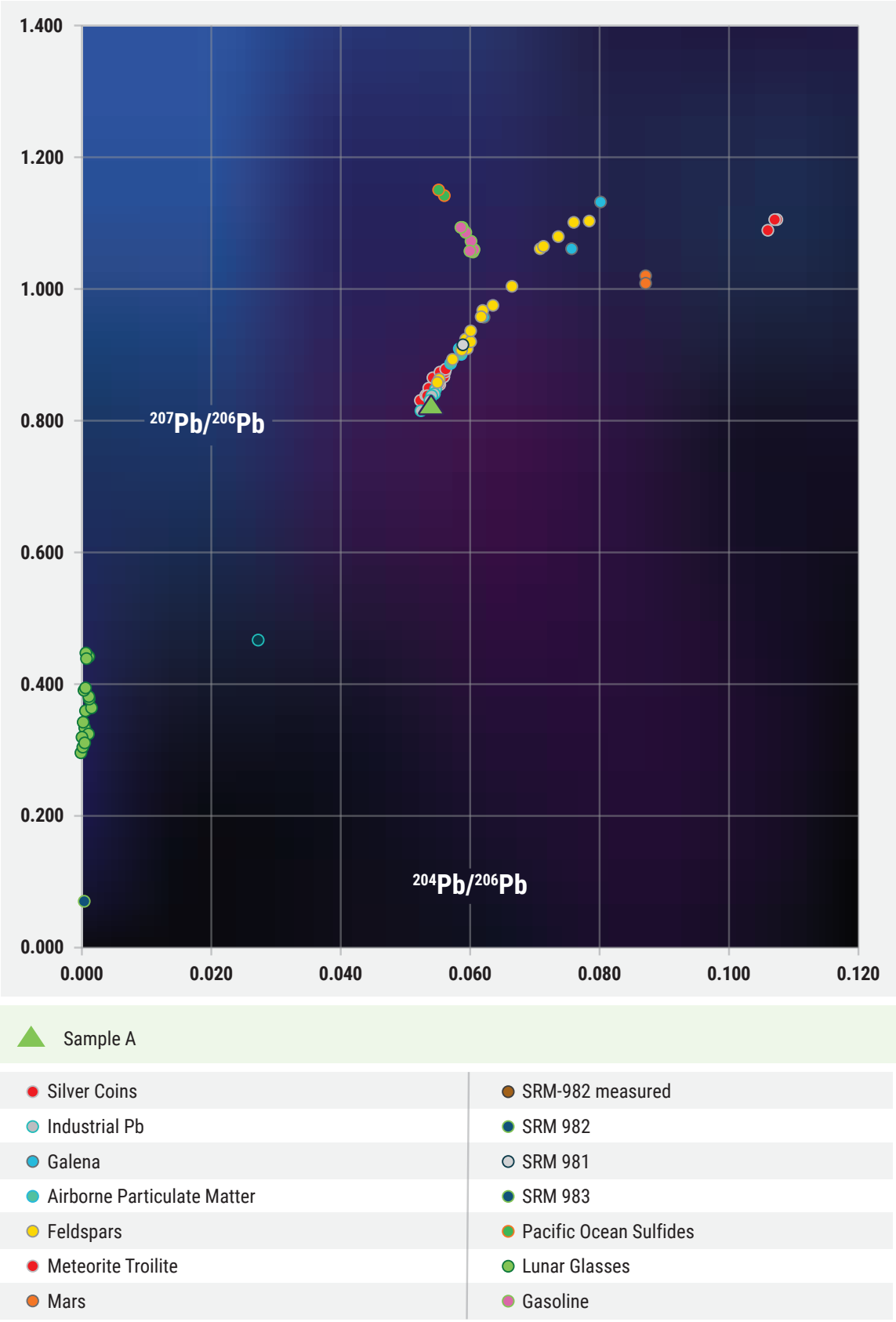

Figure 7. Lead (Pb) isotope systematics of the unknown material, shown relative to other terrestrial and non-terrestrial materials in $^{206}Pb/^{204}Pb$ vs. $^{207}Pb/^{206}Pb$. This plot has three end-member compositions: (1) primordial lead, which is the starting composition of the lead in the solar system; (2) pure radiogenic lead from the decay of naturally occurring uranium; and (3) terrestrial lead or "common lead," which is defined by repeat analyses. The specimen has a lead isotopic composition that plots precisely in the field of terrestrial lead compositions. SRM stands for standard reference material, materials typically used to perform instrument calibrations due to their well-characterized composition or properties, as measured and certified by the U.S. Department of Commerce's National Institute for Standards and Technology.

Conclusion

AARO secured ORNL to independently assess the requirements necessary to confirm or contest public claims that this historical specimen is of non-terrestrial origin and that it is capable of functioning as a bismuth-based terahertz waveguide. Although the origin, chain of custody, and ultimate purpose of this specimen remain unclear, a modern and robust analysis of its chemical and structural composition and properties does not indicate that its origin is non-terrestrial, nor do the data indicate that the material examined ever had the pure single-crystalline bismuth layer that could possibly have acted as a terahertz waveguide. The intended or actual past use of the material remains undetermined, but ORNL has a high level of confidence that all data indicate the material was manufactured terrestrially—albeit using an uncommon mixture of elements by today's standards—and then incurred damage caused by mechanical and heat stressors.

References

1. Akram, W.; Schönbächler, M., Zirconium isotope constraints on the composition of Theia and current Moon-forming theories. Earth Planet Sc Lett **2016**, 449, 302-310.
2. Albarede, F.; Blichert-Toft, J.; Gentelli, L.; Milot, J.; Vaxevanopoulos, M.; Klein, S.; Westner, K.; Birch, T.; Davis, G.; de Callataÿ, F., A miner's perspective on Pb isotope provenances in the Western and Central Mediterranean. J Archaeol Sci **2020**, 121.
3. Blichert-Toft, J.; Zanda, B.; Ebel, D. S.; Albarède, F., The Solar System primordial lead. Earth Planet Sc Lett **2010**, 300 (1-2), 152-163.
4. Budde, G.; Tissot, F. L. H.; Kleine, T.; Marquez, R. T., Spurious molybdenum isotope anomalies resulting from non-exponential mass fractionation. Geochemistry-Germany **2023**, 83 (3).
5. Catanzaro, E. J.; Murphy, T. J.; Shields, W. R.; Garner, E. L., Absolute Isotopic Abundance Ratios of Common Equal-Atom and Radiogenic Lead Isotopic Standards. J Res Nbs a Phys Ch **1968**, A 72 (3), 261-+.
6. Chakrabarti, R.; Jacobsen, S. B., The isotopic composition of magnesium in the inner Solar System. Earth Planet Sc Lett **2010**, 293 (3-4), 349-358.
7. Connelly, J. N.; Bizzarro, M.; Thrane, K.; Baker, J. A., The pb-pb age of angrite SAH99555 revisited. Geochim Cosmochim Ac **2008**, 72 (19), 4813-4824.
8. de Vega, C. G.; Chernonozhkin, S. M.; Grigoryan, R.; Costas-Rodríguez, M.; Vanhaecke, F., Characterization of the new isotopic reference materials IRMM-524A and ERM-AE143 for Fe and Mg isotopic analysis of geological and biological samples. J Anal Atom Spectrom **2020**, 35 (11), 2517-2529.
9. Fouquet, Y.; Marcoux, E., Lead-Isotope Systematics in Pacific Hydrothermal Sulfide Deposits. J Geophys Res-Sol Ea **1995**, 100 (B4), 6025-6040.
10. Gyngard, K. M. H. a. F., The Presolar Grain Database. In 40th Lunar and Planetary Science Conference, **2009**.
11. Higgins, J. A.; Schrag, D. P., Records of Neogene seawater chemistry and diagenesis in deep-sea carbonate sediments and pore fluids. Earth Planet Sc Lett **2012**, 357, 386-396.
12. Hoppe, P.; Leitner, J.; Kodolányi, J.; Vollmer, C., Isotope Systematics of Presolar Silicate Grains: New Insights from Magnesium and Silicon. Astrophys J **2021**, 913 (1).
13. Hulston, J. R.; Thode, H. G., Variations in S33 S34 and S36 Contents of Meteorites and Their Relation to Chemical and Nuclear Effects. J Geophys Res **1965**, 70 (14), 3475-+.
14. Kammerer, C. C.; Kulkarni, N. S.; Warmack, R. J.; Sohn, Y. H., Interdiffusion and impurity diffusion in polycrystalline Mg solid solution with Al or Zn. J Alloy Compd **2014**, 617, 968-974.
15. Karl K. Turekian, H. D. H., Presolar Grains. In Treatise on Geochemistry, 2 ed.; **2013**.
16. Kodolányi, J.; Hoppe, P.; Gröner, E.; Pauly, C.; Mücklich, F., The Mg isotope composition of presolar silicate grains from red giant stars. Geochim Cosmochim Ac **2014**, 140, 577-605.
17. Leitner, J.; Hoppe, P., A new population of dust from stellar explosions among meteoritic stardust. Nat Astron **2019**, 3 (8), 725-729.
18. Leonid V. Alekseyev, V. A. P., and Evgenii E. Narimanov, Homogeneous Hyperbolic Systems for Terahertz and Far-Infrared Frequencies. Advances in OptoElectronics **2012**, (Modern Trends in Metamaterial Applications), 6.
19. Liu, N.; Dauphas, N.; Cristallo, S.; Palmerini, S.; Busso, M., Oxygen and aluminum-magnesium isotopic

systematics of presolar nanospinel grains from CI chondrite Orgueil. Geochim Cosmochim Ac **2022**, 319, 296-317.
20. Lubecke, V. M.; Mizuno, K.; Rebeiz, G. M., Micromachining for terahertz applications. LEEE T Microw Theory **1998**, 46 (11), 1821-1831.
21. Monna, F.; Lancelot, J.; Croudace, I. W.; Cundy, A. B.; Lewis, J. T., Pb isotopic composition of airborne particulate material from France and the southern United Kingdom: Implications for Pb pollution sources in urban areas. Environ Sci Technol **1997**, 31 (8), 2277-2286.
22. Moriwaki, R.; Usui, T.; Tobita, M.; Yokoyama, T., Geochemically heterogeneous Martian mantle inferred from Pb isotope systematics of depleted shergottites. Geochim Cosmochim Ac **2020**, 274, 157-171.
23. Nemchin, A. A.; Whitehouse, M. J.; Grange, M. L.; Muhling, J. R., On the elusive isotopic composition of lunar Pb. Geochim Cosmochim Ac **2011**, 75 (10), 2940-2964.
24. Nguyen, A. N.; Messenger, S., Resolving the Stellar Sources of Isotopically Rare Presolar Silicate Grains through Mg and Fe Isotopic Analyses. Astrophys J **2014**, 784 (2).
25. Patterson, C., Age of Meteorites and the Earth. Geochim Cosmochim Ac **1956**, 10 (4), 230-237.
26. Rutledge, D. B.; Schwarz, S. E.; Hwang, T. L.; Angelakos, D. J.; Mei, K. K.; Yokota, S., Antennas and Wave-Guides for Far-Infrared Integrated-Circuits. LEEE J Quantum Elect **1980**, 16 (5), 508-516.
27. Song, Q.; Chen, H.; Zhang, M.; Li, L.; Yang, J. B.; Yan, P. G., Broadband electrically controlled bismuth nanofilm THz modulator. Apl Photonics **2021**, 6 (5).
28. Stacey, J. S.; Kramers, J. D., Approximation of Terrestrial Lead Isotope Evolution by a 2-Stage Model. Earth Planet Sc Lett **1975**, 26 (2), 207-221.
29. Steele, R. C. J.; Elliott, T.; Coath, C. D.; Regelous, M., Confirmation of mass-independent Ni isotopic variability in iron meteorites. Geochim Cosmochim Ac **2011**, 75 (24), 7906-7925.
30. Sturrock, P., Composition analysis of the Brazil magnesium. Journal of Scientific Exploration **2001**, 15 (1), 69-95.
31. Tatsumoto, M.; Knight, R. J.; Allegre, C. J., Time Differences in Formation of Meteorites as Determined from Ratio of Pb-207 to Pb-206. Science **1973**, 180 (4092), 1279-1283.
32. Teng, F. Z., Magnesium Isotope Geochemistry. Rev Mineral Geochem **2017**, 82, 219-287.
33. Timmes, F. X.; Woosley, S. E.; Weaver, T. A., Galactic Chemical Evolution - Hydrogen through Zinc. Astrophys J Suppl S **1995**, 98 (2), 617-658.
34. Vermeesch, P., IsoplotR: A free and open toolbox for geochronology. Geosci Front **2018**, 9 (5), 1479-1493.
35. Wakaki, S.; Tanaka, T., Stable isotope analysis of Nd by double spike thermal ionization mass spectrometry. Int J Mass Spectrom **2012**, 323, 45-54.
36. Wang, T.; Schwarz, S. E., Design of Dielectric Ridge Waveguides for Millimeter-Wave Integrated-Circuits. LEEE T Microw Theory **1983**, 31 (2), 128-134.
37. White, W. M., Chapter 8: Stable Isotope Theory. In Isotope Geochemistry, **2014**; p 720.
38. Wombacher, F.; Eisenhauer, A.; Heuser, A.; Weyer, S., Separation of Mg, Ca and Fe from geological reference materials for stable isotope ratio analyses by MC-ICP-MS and double-spike TIMS. J Anal Atom Spectrom **2009**, 24 (5), 627-636.
39. Young, E. D.; Galy, A., The isotope geochemistry and cosmochemistry of magnesium. Geochemistry of Non-Traditional Stable Isotopes **2004**, 55, 197-230.
40. Young, E. D.; Galy, A.; Nagahara, H., Kinetic and equilibrium mass-dependent isotope fractionation laws in nature and their geochemical and cosmochemical significance. Geochim Cosmochim Ac **2002**, 66 (6), 1095-1104.